www.sciencemag.org/345/6198/786/suppl/DC1

Supplementary Materials for

Evidence for interstellar origin of seven dust particles collected by the Stardust spacecraft

Andrew J. Westphal,* Rhonda M. Stroud, Hans A. Bechtel, Frank E. Brenker, Anna L. Butterworth, George J. Flynn, David R. Frank, Zack Gainsforth, Jon K. Hillier, Frank Postberg, Alexandre S. Simionovici, Veerle J. Sterken, Larry R. Nittler, Carlton Allen, David Anderson, Asna Ansari, Saša Bajt, Ron K. Bastien, Nabil Bassim, John Bridges, Donald E. Brownlee, Mark Burchell, Manfred Burghammer, Hitesh Changela, Peter Cloetens, Andrew M. Davis, Ryan Doll, Christine Floss, Eberhard Grün, Philipp R. Heck, Peter Hoppe, Bruce Hudson, Joachim Huth, Anton Kearsley, Ashley J. King, Barry Lai, Jan Leitner, Laurence Lemelle, Ariel Leonard, Hugues Leroux, Robert Lettieri, William Marchant, Ryan Ogliore, Wei Jia Ong, Mark C. Price, Scott A. Sandford, Juan-Angel Sans Tresseras, Sylvia Schmitz, Tom Schoonjans, Kate Schreiber, Geert Silversmit, Vicente A. Solé, Ralf Srama, Frank Stadermann, Thomas Stephan, Julien Stodolna, Stephen Sutton, Mario Trieloff, Peter Tsou, Tolek Tyliszczak, Bart Vekemans, Laszlo Vincze, Joshua Von Korff, Naomi Wordsworth, Daniel Zevin, Michael E. Zolensky, 30714 Stardust@home dusters

*Corresponding author. E-mail: westphal@ssl.berkeley.edu

Published 15 August 2014, *Science* **345**, 786 (2014)
DOI: 10.1126/science.1252496

This PDF file includes:

Materials and Methods

The methods and measurements are described in detail in the series of supporting papers published contemporaneously with this article (*9-20*).

Table S1. Criteria for Classification of Captured Candidate Interstellar Particles.

	Aerogel	Al Foil
Level 0	Impact-like feature in aerogel	Impact-like feature in the foil
Level 1	Track or impact feature definitively confirmed by high-resolution optical microscopy	Impact crater confirmed by scanning electron microscopy
Level 2	Trajectory consistent with interstellar origin and composition inconsistent with spacecraft materials	Residue composition inconsistent with spacecraft materials
Level 3	O isotope composition inconsistent with solar values	O isotope composition inconsistent with solar values

Supplementary Text

1. Backgrounds

The two sources of background in the search for interstellar dust particles are interplanetary dust particles and particles in the secondary ejecta from micrometeoroid impacts on the spacecraft that are dominated by extraterrestrial projectile material. We have presented assessments of both background sources in (*10*), but expand on them here.

To assess the probability that the three interstellar candidates in aerogel have an interplanetary rather than interstellar origin, we used our observation of zero interplanetary dust particles in the range of azimuth angles that mostly excludes secondary ejecta from impacts on the SRC deck or on the solar panels. We test the hypothesis that three interplanetary dust particles, following the distribution shown in Fig. 2 of Frank et al. *(10),* would fall into the azimuth range consistent with an origin in the interstellar dust stream. Using a Monte Carlo simulation, we find that this probability is less than ~3×10^{-4}. Distributions for inclination and eccentricity for the Monte Carlo simulation of IDP trajectories were taken from the model of Nesvorny (*46*). Semi-minor axes were not given in that paper, but we found that the results were insensitive to the distribution of semi-minor axis. In Fig. 2 of Frank et al. (*10*) we assumed a uniform distribution of semi-major axis from 3 AU to 9 AU. We assumed an equal probability of

capture for each of the 195 days of the exposure, and an equal probability of capture for inbound or outbound sections of the orbit. We also note that the 99% of the interplanetary micrometeoroids observed in the Monte Carlo simulation were captured at speeds > 7.5 km sec^{-1}, which appears to be inconsistent with the low capture speeds of Orion and Hylabrook.

Asteroidal dust is a possible source of background in the identification of interstellar dust. Nesvorny et al. (*46*) found that the fraction of interplanetary dust that has an asteroidal origin is <15% within 10º of the ecliptic, and that most interplanetary dust has a cometary origin, which we modeled by Monte Carlo (Fig. 2 of Frank et al.). Thus, our upper limit on interplanetary cometary dust gives an even stricter upper limit on asteroidal dust, by at least a factor of six.

To investigate this possibility further, we performed Monte Carlo simulations of capture trajectories of asteroidal dust in the collector. The two largest populations of asteroidal dust are the Karin and Veritas populations (*47*). We used the approximate distributions of eccentricity, semi-major axis and inclination for these two populations given by Nesvorny et al. (*47*). In both cases, all 10,000 simulations of particle trajectories appeared at azimuths far from those of the three candidates in aerogel, and in the opposite hemisphere of the sky (Figs. S1 and S2). Simulations of dust impacts from rare, so-called main-belt comets (Jewitt et al.) (*48*), Hsieh et al. (*49*)) give similar results. We also carried out a Monte Carlo simulation of the impact directions of hypothetical particles ejected from 1087 Main Belt asteroids, taken from the SKADS catalog (*50*). The trajectories are shown in Fig. S3. 2.0% of the simulations fall in the azimuth range consistent with the three candidates in aerogel, so the probability that all three candidates in aerogel are drawn from this distribution is 8×10^{-6}. Azimuth angle measurements were conducted on the particle tracks before extraction of the tracks from the aerogel tiles, and before extraction of the tiles from the tray. We monitored changes in zenith angle during tile or picokeystone extraction using fixed artificial reference tracks in the same picokeystones. In all cases errors in trajectory measurements were negligible compared with spacecraft wobble.

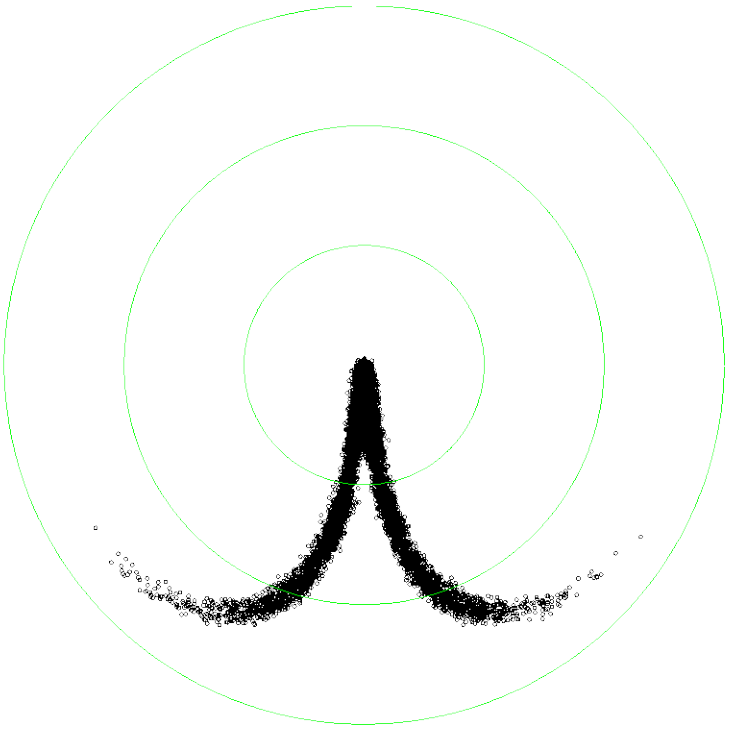

Fig. S1. Monte Carlo simulations of the trajectories of asteroidal particles from the Karin population. The coordinate system is identical to Fig. 2 of Frank et al. (*10*): The green contours are at 30º, 60º and 90º; the sunward direction is up.

Fig. S2. Monte Carlo simulations of the trajectories of asteroidal particles from the Veritas population. The coordinate system is identical to Fig. 2 of Frank et al. (*10*): The green contours are at 30º, 60º and 90º; the sunward direction is up.

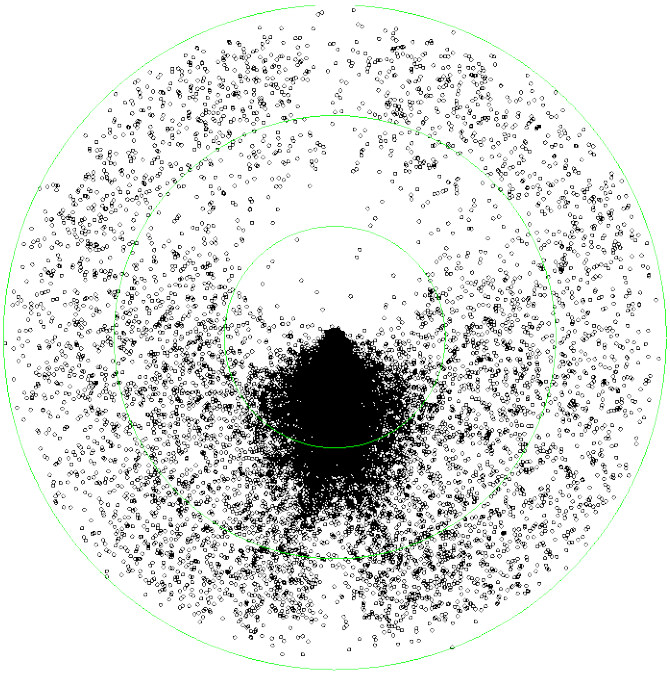

Fig. S3. Monte Carlo simulations of the trajectories of hypothetical asteroidal particles released from 1087 Main Belt asteroids, taken from the SKADS catalog (*50*). The coordinate system is identical to Fig. 2 of Frank et al. (*10*): The green contours are at 30º, 60º and 90º; the sunward direction is up.

In the assessment of the background due to secondary ejecta in (*10*), we assumed an asymptotically large exposure factor on the spacecraft, so that the entire interplanetary dust spectrum was sampled. The probability distribution of the target/projectile (T/P) ratio in the ejecta is a strong function of interplanetary dust fluence: for small fluences, ejecta from impacts of small projectiles dominate, so a small T/P ratio is most likely, while for sufficiently large exposures, ejecta from relatively rare large projectiles dominate, resulting in large T/P ratios as the most probable. Here we calculate the statistical likelihood that the interstellar dust candidates consist of secondary particles, using an estimate of the finite fluence of interplanetary dust particles on the spacecraft.

The Interplanetary Micrometeoroid Environment Model (IMEM) code is a tool that predicts micrometeoroid fluence with a defined size range, on a surface with a defined orientation, over a defined segment of a Keplerian orbit (*32*). We used IMEM to calculate the fluence of micrometeoroids on the deck of the Stardust Sample Return Capsule for the two collection periods. The result was 116 impacts greater than 1 pg. We scaled this result to that of the Grün model (*51*) for a rotating flat plate at 1AU, which gives 263 such impacts. Thus the SRC deck would have received about 44% of the nominal fluence predicted by the Grün model. IMEM also predicted an average impact speed of ~10 km s^{-1} , instead of 12 km s^{-1} in our simulation based on Nesvorny et al. (*47*). We thus assumed 10 km s^{-1} average impact speed in subsequent calculations because it tends to give a lower target/projectile ratio, which is the more conservative assumption. We

then used a Monte Carlo simulation to calculate the median and 2σ lower limits on the T/P mass ratio in the ejecta, as a function of micrometeoroid fluence, normalized to the prediction of the Grün model. To compute the T/P ratio for each projectile in the Monte Carlo simulation, we used the observations of crater diameters in aluminum targets as a function of projectile size, reported by Price et al. (*23*). We assumed that the amount of ejected target material was proportional to the crater volume, and we assumed that the target material and projectile material were ejected from the impact with equal efficiency. We then compared this to the 2-σ upper limit on the target/projectile ratio for tracks in aerogel and craters in foils. Fig. S4 shows the result. The solid line is the median T/P ratio as a function of micrometeoroid fluence, in units of the Grün model prediction, the dashed line is the 2σ lower limit, and the solid blue and red lines are the 2σ upper limits from the track and crater statistics. The green line is the IMEM prediction. We conclude that the actual micrometeoroid fluence is a factor of two greater than the maximum fluence on the SRC that gives consistency at the ≤3σ level in the T/P ratio between the Monte Carlo simulation and the observations in the aerogel. Since the solar panels are so much larger than the SRC, this factor is even greater for the craters. We conclude that the observed T/P ratio is inconsistent with a secondary origin for the interstellar candidates in either aerogel or foils.

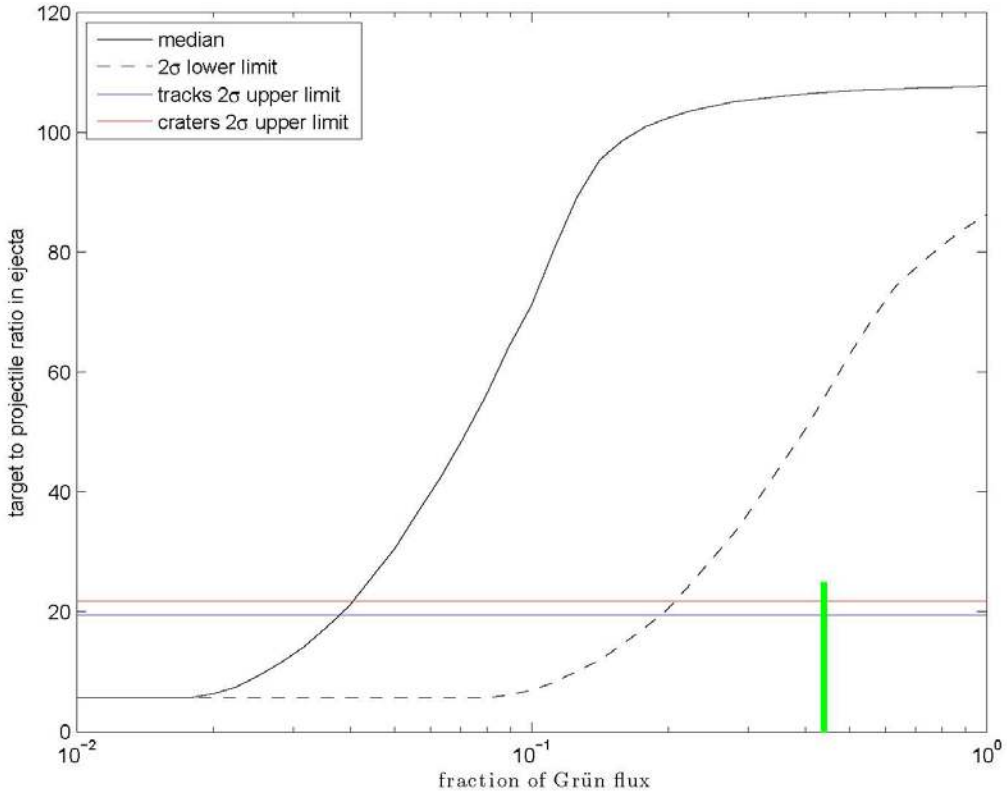

Fig. S4. Monte Carlo simulations of the target/projectile mass ratio in the ejecta of micrometeoroid impacts on the Stardust Sample Return Capsule deck, as a function of micrometeoroid fluence, normalized to the prediction of the Grün model for particles > 10 μm. The green line indicates the fluence received by Stardust as predicted by IMEM.

We also explored the possibility that the ejection of target material was suppressed relative to the projectile material for small projectiles. For projectiles larger than 10µm in diameter, cratering seems to be self-similar on all scales, but self-similarity breaks down for polycrystalline Al targets and projectiles near to or smaller than the Al crystallite grain size. Because we have no experimental information about the relative ejection rates of target and projectile material, we took a conservative approach, and assumed that below 10µm, no target material is ejected, and all the projectile material is ejected. Fig. S5 shows the result. Although the curve shows the effects of this assumption at low fluence, there is no change in the general conclusion.

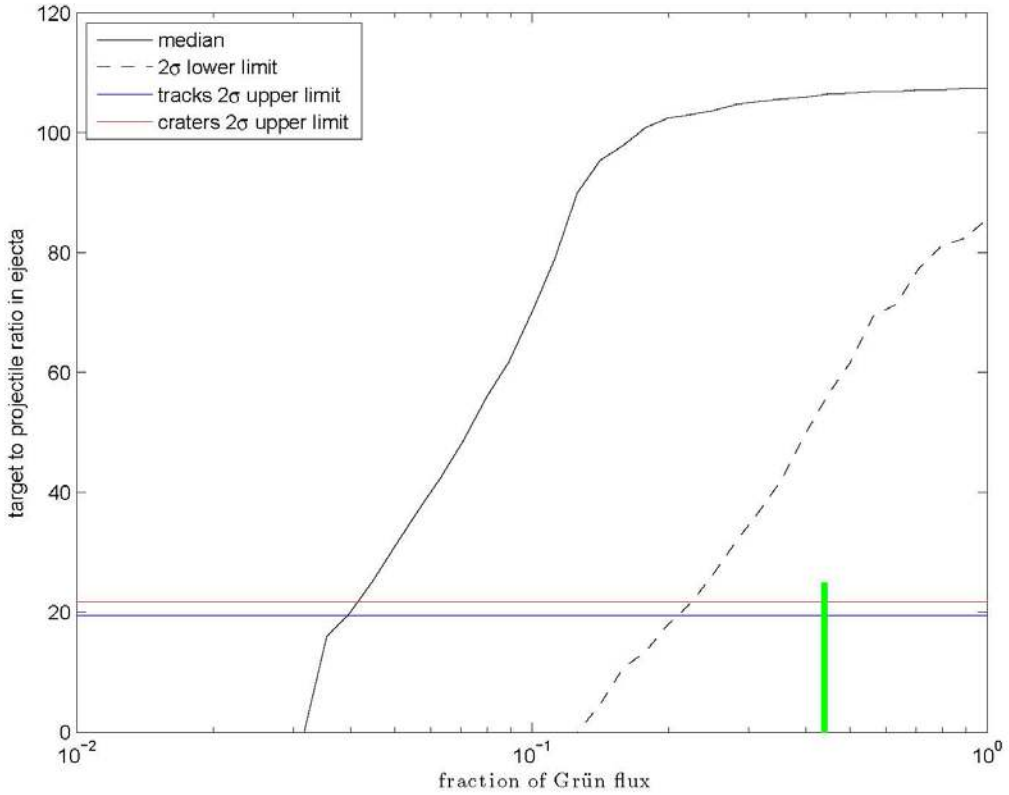

Fig. S5. Monte Carlo simulations of the target/projectile mass ratio in the ejecta of micrometeoroid impacts on the Stardust Sample Return Capsule deck, as a function of micrometeoroid fluence, normalized to the prediction of the Grün model (*51*) for particles > 10 µm. The green line indicates the fluence received by Stardust as predicted by IMEM. Here we assume that no target material is ejected for impacts of projectiles < 10 µm in diameter.

2. STEM analyses of crater residues

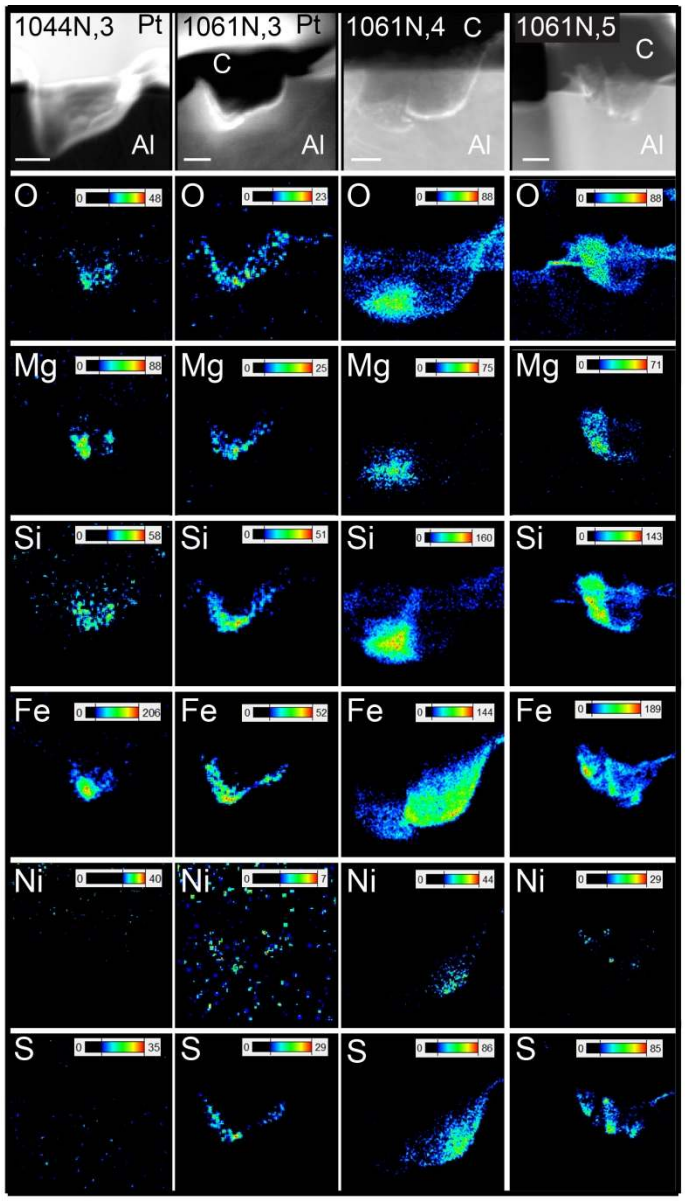

Fig. S6. Dark field STEM images (top row) and net-count EDS element maps of the four candidate interstellar dust impact residues in Al foil. Scale bars indicate 100 nm. Pt and C refer to FIB-deposited protective masks.

Figure S6 shows the spatial distribution of the elemental components in the impact crater residues, extracted from STEM-EDS spectrum images. 1044N,3 shows clear zoning of the Mg, Si and Fe contents, but is a single particle. 10661N,3 shows mixed silicate and sulfide components, indicating a single particle or fine-grained aggegrate. 1061N,4 shows zoning into two components > 100 nm, one silicate and one sulfide, consistent with the

double-bowl shape of the crater that indicates two mass centers. 1061N,5 also shows distinct silicate and sulfide components, but the Ni and S distribution indicate that the sulfide consisted of multiple particles < 10 nm.

3. Crater oxygen isotope measurements

We used secondary ion mass spectrometry to measure O isotopes on Focused-Ion Beam (FIB) cross-sections of two candidate interstellar impact craters, one crater found to contain residue from solar panel cover glass, and two similarly sized impact craters from the Stardust Wild 2 cometary Al-foil collection (*19*). In order to minimize instrumental artifacts associated with measurements of cross-sections suspended on Omniprobe grids, the crater FIB sections were first removed from TEM Omniprobe grids, transferred to clean Au foils and coated with a thin Au coat as described in (*19*). Analyses were carried out with a Cameca NanoSIMS 50L ion microprobe at the Carnegie Institution of Washington. A <1 pA, ~100 nm diameter Cs^+ primary ion beam was rastered (128×128 pixel, 16–25μm^2) over each sample and negative secondary ions of $^{12,13}C$, $^{16,17,18}O$, ^{28}Si, and $^{27}Al^{16}O$ were simultaneously collected along with secondary electrons in multicollection imaging mode, with total dwell times of ~0.25 seconds per pixel. The cometary craters, solar cell glass crater and contamination present in all samples were used to correct for instrumental mass fractionation and possible different detection efficiencies of the electron multipliers used to detect the secondary ions. Isotopic images were quantitatively analyzed with the L'image software (L. Nittler, CIW). Errors are completely dominated by counting statistics. Figure S7 shows NanoSIMS images for the two interstellar candidate craters; crater residue is clearly resolvable.

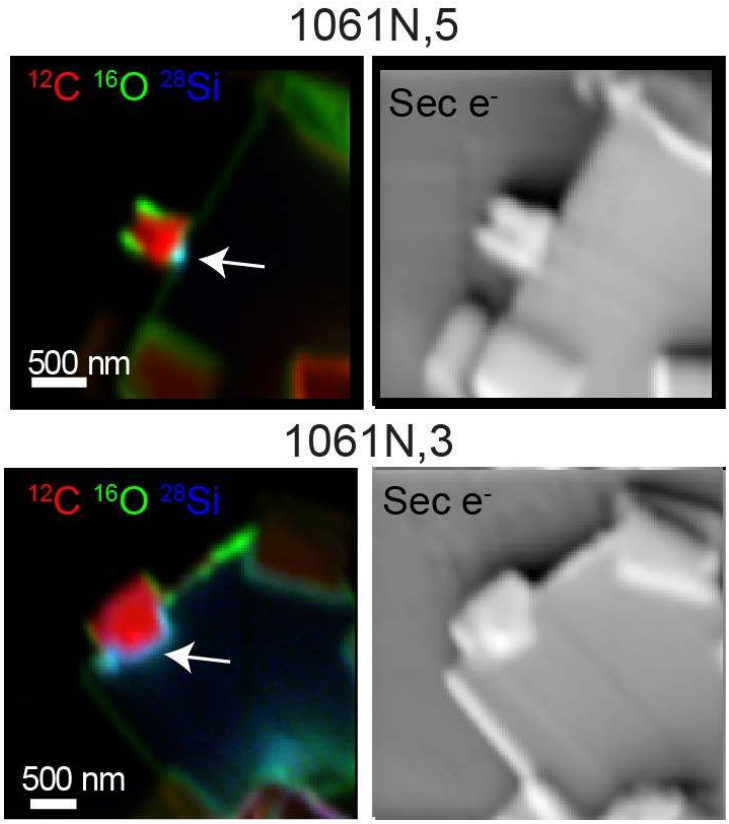

Fig. S7. NanoSIMS images of two interstellar candidate crater FIB cross-sections. Left panels indicate red-green-blue overlays of signals from ^{12}C, ^{16}O, and ^{28}Si, respectively, while right panels show the corresponding secondary electron images. Arrows indicate crater residues.

Derived oxygen isotope ratios are shown in Figures S8 and S9. The interstellar candidate residues have oxygen isotope ratios indistinguishable from those of the cometary and solar panel glass residues and contamination on the samples. O-rich presolar circumstellar grains in meteorites and comet samples have very large O-isotopic anomalies [e.g. refs *30*, *43*, *44*] such that they typically plot outside of the range of Fig S8. The measured compositions for the residues hence are clearly incompatible with a stellar origin. However, even grains formed in the ISM may have non-solar O isotopic ratios. For example, radio telescopic measurements of molecular clouds throughout the Galaxy have revealed them to typically have lower $^{18}O/^{17}O$ ratios (~4.1) than the Solar System value of 5.2 (Figs. S8 and S9). Recent infrared measurements of a few young stellar objects have found similar non-solar $^{18}O/^{17}O$ ratios (*52*). The origin of the oxygen isotopic discrepancy between much of the present-day Milky Way interstellar medium and the Solar System is controversial, and both supernova injection into the Sun's parental molecular cloud (*53*) and the chemical evolution of the Galaxy in the 4.6 Ga since solar birth (*54*) have been proposed. The interstellar observations would seem to indicate that interstellar dust forming today in the ISM should have lower-than-solar $^{18}O/^{17}O$ ratios on average, in contrast with our two candidate crater measurements. However, the molecular cloud observations show considerable scatter, for example one

cloud at the Sun's galactocentric radius is seen to have a solar-like $^{18}O/^{17}O$ ratio (arrow, Fig. S9). The oxygen isotopic composition of the local ISM from which our candidate particles may have originated has not been directly measured, and it is thus possible that it has a solar-like composition. The normal oxygen isotopic composition measured in the two crater residues therefore does not rule out an interstellar origin.

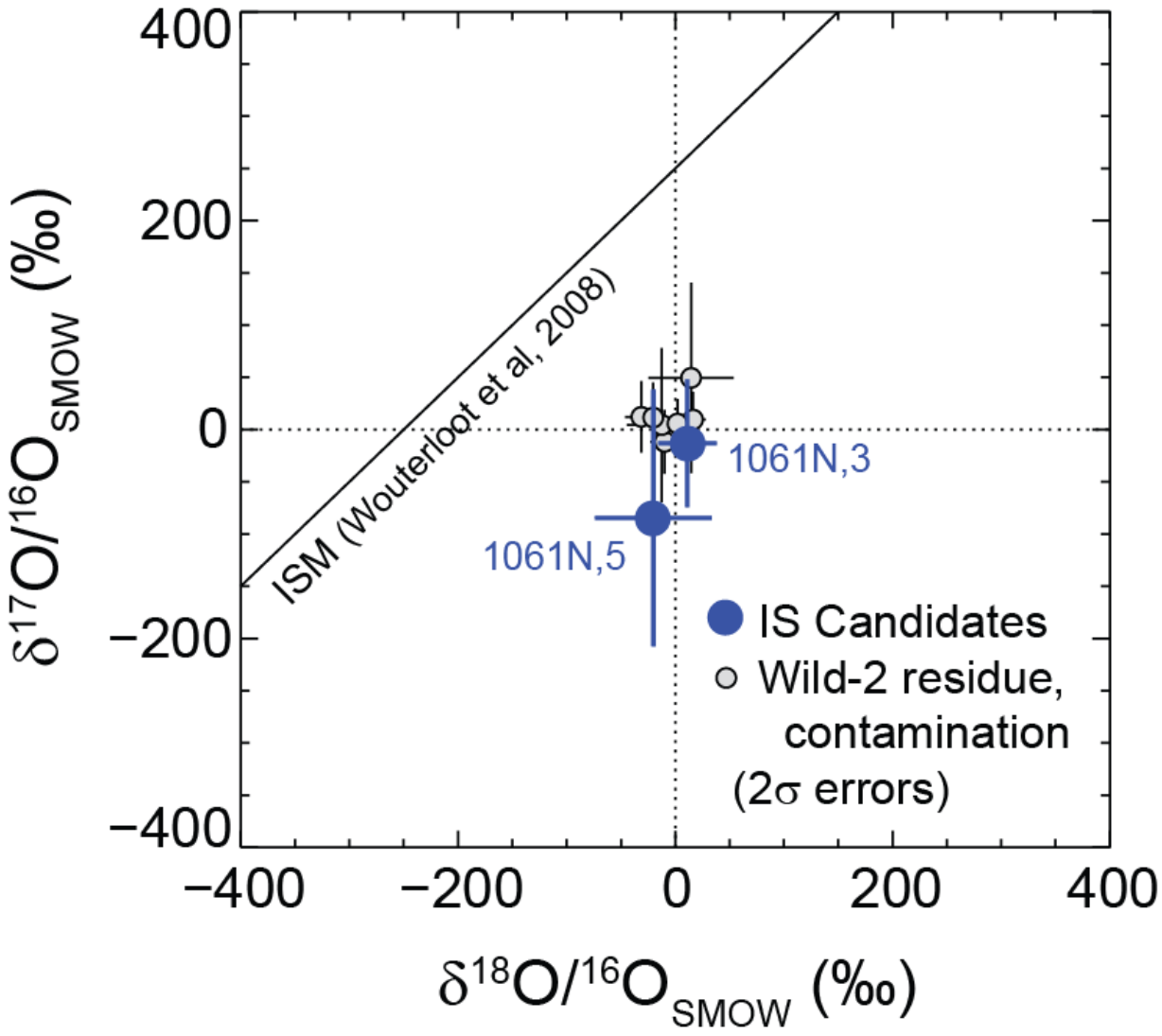

Fig. S8. Oxygen 3-isotope plot for candidate interstellar crater residues and other measured samples. Isotopic ratios are given as delta-values, ‰ deviations from Standard Mean Ocean Water (SMOW), represented by dotted lines. All measured values are within errors of terrestrial and distinct from the average composition of molecular clouds as determined by astronomical observations (*55*).

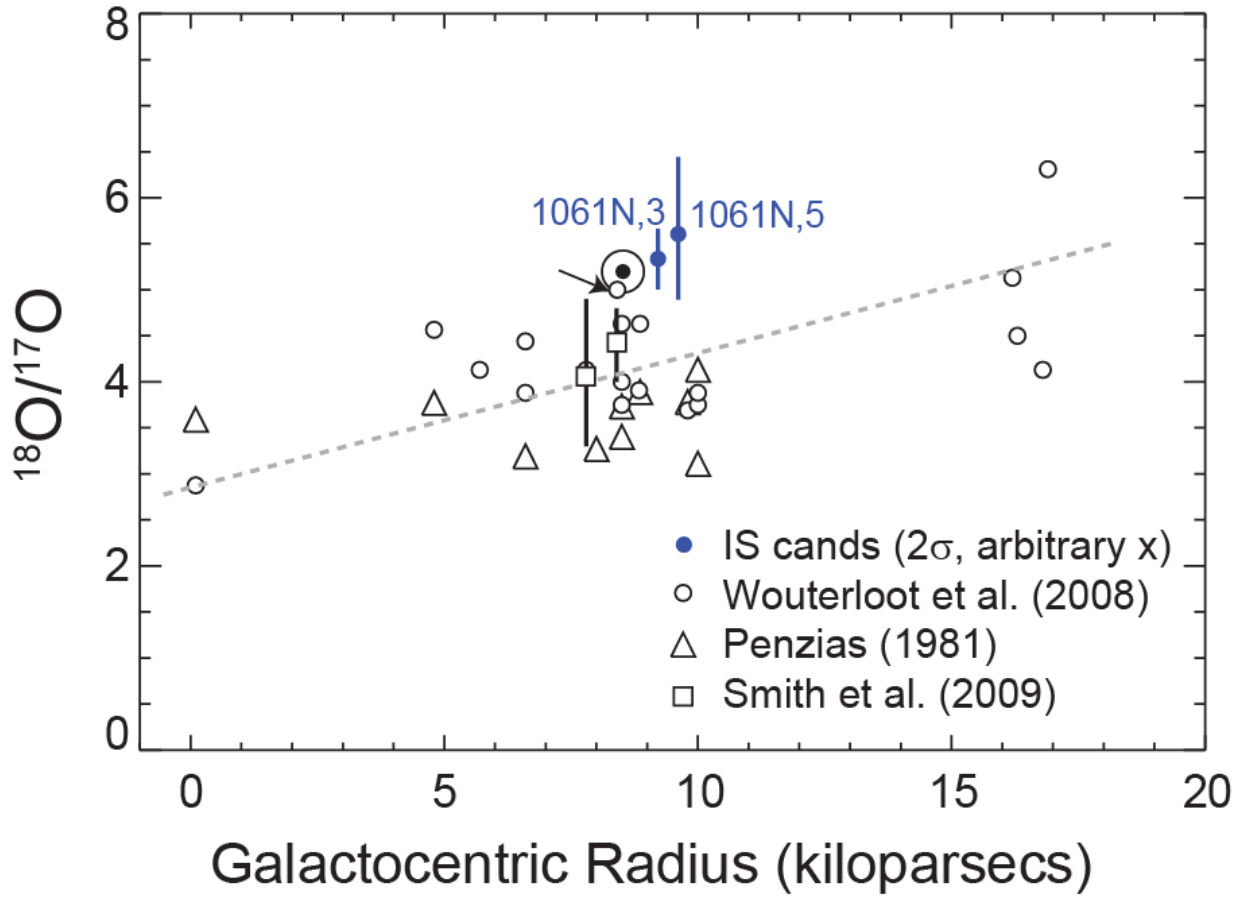

Fig. S9. $^{18}O/^{17}O$ ratios of two interstellar candidate crater residues (blue symbols, plotted at arbitrary abscissa values) are compared to astronomical measurements of molecular clouds (open circles and triangles, (*56*) and (*55*)) and young stellar objects (squares, (*52*)). Dashed line indicates possible galactic gradient in $^{18}O/^{17}O$ ratio suggested by Wouterloot et al. data (*55*). Arrow indicates one molecular cloud with solar-like $^{18}O/^{17}O$ ratio. After Nittler and Gaidos (*54*).

3. Composition of Orion

The oxidation state of Fe in Orion is unknown, resulting in an uncertainty in stoichiometric oxygen, hence there are uncertainties in the bulk atomic fractions and total mass of the particle (Table S.2) and in estimation of the fraction of Orion's molecular phases (Table S.3). We assumed stoichiometric forsteritic olivine (Mg_2SiO_4), spinel ($MgAl_2O_4$) and S occurred as FeS, but we do not imply that these phases were present as crystalline minerals in Orion. Based on XRD evidence that one Fe phase is consistent with Fe nanoparticles, we favor the assumption that the major Fe phase is Fe/FeO (some mix of Fe^0 and Fe^{2+}). The major phase composition is thus: Mg_2SiO_4 19.2±3.3 mol%, $MgAl_2O_4$ 27.5±2.3 mol% and Fe/FeO 44.7±3.5 mol%. In Table S.3 we show the effect on the bulk molecular fractions if the non-sulfide Fe was completely oxidized to Fe_2O_3.

Table S2. Elemental composition of Orion depending on Fe oxidation state.

Element	Measured Mass femtogram	Atomic Fraction Reduced Fe	Atomic Fraction (FeO) Fe^{2+}	Atomic Fraction (Fe_2O_3) Fe^{3+}
Mg (olivine)	300 ±60	10.1±2.0 %	8.9±1.8 %	8.5 %
Mg (spinel)	200 ±40	6.7±1.3 %	6.0±1.2 %	5.7 %
Al	475 ±35	14.3±1.1 %	12.7±0.9 %	12.1 %
Fe	840 ±100	12.3±1.5 %	10.9±1.3 %	10.3 %
S	23 ±10%	0.6±0.12 %	0.5±0.1 %	0.5 %
Ca	23 ±10%	0.5±0.05 %	0.4±0.04 %	0.4 %
Cr	12 ±10%	0.2±0.02 %	0.2±0.02 %	0.2 %
Mn	14 ±10%	0.2 ±0.02 %	0.2±0.02 %	0.2 %
Ni	55 ±10%	0.08±0.08 %	0.7±0.07 %	0.6 %
Cu	11 ±10%	0.1±0.01 %	0.1±0.01 %	0.1 %
Si*		*5.0 %*	*4.5 %*	*4.2 %*
O*		*49.3 %*	*54.9 %*	*57.2 %*
Total Particle Mass		3.1 pg	3.3 pg	3.4 pg

* Si and O are assigned stoichiometrically without implying that phases are crystalline.

Table S3. Bulk molecular phases in Orion, varying the unknown Fe phase.

Phase	Molar fraction Fe metal	Molar fraction FeO	Molar fraction Fe_2O_3
Forsterite (Mg_2SiO_4)	19.2±3.3 %	19.2±3.3 %	24.8 %
Spinel ($MgAl_2O_4$)	27.5±2.3 %	27.5±2.3 %	35.3 %
Major Fe phase	44.7± 3.5% (Fe)	44.7± 3.5% (FeO)	28.8 % (Fe_2O_3)
Minor reduced phases	5.7 % (FeS, Ni, Cu)	2.2 % (FeS)	2.9 % (FeS)
Minor oxides	2.9±0.3 % (CaO, Cr_2O_3, MnO)	6.4±0.6 % (CaO, Cr_2O_3, MnO, NiO, CuO)	8.2 % (CaO, Cr_2O_3, MnO, NiO, CuO)

References and Notes

1. P. C. Frisch, J. D. Slavin, Interstellar dust close to the Sun. *Earth Planets Space* **65**, 175–182 (2013). doi:10.5047/eps.2012.05.001

2. H. Kimura, I. Mann, E. K. Jessberger, Composition, structure, and size distribution of dust in the local interstellar cloud. *Astrophys. J.* **583**, 314–321 (2003). doi:10.1086/345102

3. B. T. Draine, Interstellar dust grains. *Annu. Rev. Astron. Astrophys.* **41**, 241–289 (2003). doi:10.1146/annurev.astro.41.011802.094840

4. M. Landgraf, W. J. Baggaley, E. Grun, H. Kruger, G. Linkert, Aspects of the mass distribution of interstellar dust grains in the solar system from in situ measurements. *J. Geophys. Res. Space Phys.* **105**, 10343–10352 (2000). doi:10.1029/1999JA900359

5. E. Grün, H. A. Zook, M. Baguhl, A. Balogh, S. J. Bame, H. Fechtig, R. Forsyth, M. S. Manner, M. Horanyi, J. Kissel, B.-A. Lindblad, D. Linkert, G. Linkert, I. Mann, J. A. M. McDonnell, G. E. Morfill, J. L. Phillips, C. Polanskey, G. Schwehm, N. Siddique, P. Staubach, J. Svestka, A. Taylor, Discovery of Jovian Dust Streams and Interstellar Grains by the Ulysses Spacecraft. *Nature* **362**, 428–430 (1993). doi:10.1038/362428a0

6. H. Krüger, V. Dikarev, B. Anweiler, S. F. Dermott, A. L. Graps, E. Grün, B. A. Gustafson, D. P. Hamilton, M. S. Hanner, M. Horányi, J. Kissel, D. Linkert, G. Linkert, I. Mann, J. A. M. McDonnell, G. E. Morfill, C. Polanskey, G. Schwehm, R. Srama, Three years of Ulysses dust data: 2005 to 2007. *Planet. Space Sci.* **58**, 951–964 (2010). doi:10.1016/j.pss.2009.11.002

7. All particle sizes heareafter are given in diameter, rather than radius.

8. D. Brownlee, P. Tsou, J. Aléon, C. M. Alexander, T. Araki, S. Bajt, G. A. Baratta, R. Bastien, P. Bland, P. Bleuet, J. Borg, J. P. Bradley, A. Brearley, F. Brenker, S. Brennan, J. C. Bridges, N. D. Browning, J. R. Brucato, E. Bullock, M. J. Burchell, H. Busemann, A. Butterworth, M. Chaussidon, A. Cheuvront, M. Chi, M. J. Cintala, B. C. Clark, S. J. Clemett, G. Cody, L. Colangeli, G. Cooper, P. Cordier, C. Daghlian, Z. Dai, L. D'Hendecourt, Z. Djouadi, G. Dominguez, T. Duxbury, J. P. Dworkin, D. S. Ebel, T. E. Economou, S. Fakra, S. A. Fairey, S. Fallon, G. Ferrini, T. Ferroir, H. Fleckenstein, C. Floss, G. Flynn, I. A. Franchi, M. Fries, Z. Gainsforth, J. P. Gallien, M. Genge, M. K. Gilles, P. Gillet, J. Gilmour, D. P. Glavin, M. Gounelle, M. M. Grady, G. A. Graham, P. G. Grant, S. F. Green, F. Grossemy, L. Grossman, J. N. Grossman, Y. Guan, K. Hagiya, R. Harvey, P. Heck, G. F. Herzog, P. Hoppe, F. Hörz, J. Huth, I. D. Hutcheon, K. Ignatyev, H. Ishii, M. Ito, D. Jacob, C. Jacobsen, S. Jacobsen, S. Jones, D. Joswiak, A. Jurewicz, A. T. Kearsley, L. P. Keller, H. Khodja, A. L. Kilcoyne, J. Kissel, A. Krot, F. Langenhorst, A. Lanzirotti, L. Le, L. A. Leshin, J. Leitner, L. Lemelle, H. Leroux, M. C. Liu, K. Luening, I. Lyon, G. Macpherson, M. A. Marcus, K. Marhas, B. Marty, G. Matrajt, K. McKeegan, A. Meibom, V. Mennella, K. Messenger, S. Messenger, T. Mikouchi, S. Mostefaoui, T. Nakamura, T. Nakano, M. Newville, L. R. Nittler, I. Ohnishi, K. Ohsumi, K. Okudaira, D. A. Papanastassiou, R. Palma, M. E. Palumbo, R. O. Pepin, D. Perkins, M. Perronnet, P. Pianetta, W. Rao, F. J. Rietmeijer, F. Robert, D. Rost, A. Rotundi, R. Ryan, S. A. Sandford, C. S. Schwandt, T. H. See, D. Schlutter, J. Sheffield-Parker, A. Simionovici, S. Simon, I. Sitnitsky, C. J. Snead, M. K. Spencer, F. J. Stadermann, A. Steele, T. Stephan, R. Stroud, J. Susini, S. R. Sutton, Y. Suzuki, M.

Taheri, S. Taylor, N. Teslich, K. Tomeoka, N. Tomioka, A. Toppani, J. M. Trigo-Rodríguez, D. Troadec, A. Tsuchiyama, A. J. Tuzzolino, T. Tyliszczak, K. Uesugi, M. Velbel, J. Vellenga, E. Vicenzi, L. Vincze, J. Warren, I. Weber, M. Weisberg, A. J. Westphal, S. Wirick, D. Wooden, B. Wopenka, P. Wozniakiewicz, I. Wright, H. Yabuta, H. Yano, E. D. Young, R. N. Zare, T. Zega, K. Ziegler, L. Zimmerman, E. Zinner, M. Zolensky, Comet 81P/Wild 2 under a microscope. *Science* **314**, 1711–1716 (2006). Medline doi:10.1126/science.1135840

9. A. J. Westphal *et al*., Stardust Interstellar Preliminary Examination I: Identification of tracks in aerogel. *Meteorit. Planet. Sci.* 10.1111/maps.12168 (2014).

10. D. R. Frank *et al*., Stardust Interstellar Preliminary Examination II: Curating the interstellar dust collector, picokeystones, and sources of impact tracks. *Meteorit. Planet. Sci.* 10.1111/maps.12147 (2014).

11. H. A. Bechtel *et al*., Stardust Interstellar Preliminary Examination III: Infrared spectroscopic analysis of interstellar dust candidates. *Meteorit. Planet. Sci.* 10.1111/maps.12125 (2014).

12. A. L. Butterworth *et al*., Stardust Interstellar Preliminary Examination IV: Scanning Transmission X-ray Microscopy analyses of impact features in the Stardust Interstellar Dust Collector. *Meteorit. Planet. Sci.* 10.1111/maps.12220 (2014).

13. F. E. Brenker *et al*., Stardust Interstellar Preliminary Examination V: XRF analyses of interstellar dust candidates at ESRF ID13. *Meteorit. Planet. Sci.* 10.1111/maps.12206 (2014).

14. A. S. Simionovici *et al*., Stardust Interstellar Preliminary Examination VI: Quantitative elemental analysis by synchrotron X-ray fluorescence nanoimaging of eight impact features in aerogel. *Meteorit. Planet. Sci.* 10.1111/maps.12208 (2014).

15. G. J. Flynn *et al*., Stardust Interstellar Preliminary Examination VII: Synchrotron X-ray fluorescence analysis of six stardust interstellar candidates measured with the advanced photon source 2-ID-D microprobe. *Meteorit. Planet. Sci.* 10.1111/maps.12144 (2014).

16. Z. Gainsforth *et al*., Stardust Interstellar Preliminary Examination VIII: Identification of crystalline material in two interstellar candidates. *Meteorit. Planet. Sci.* 10.1111/maps.12148 (2014).

17. F. Postberg *et al*., Stardust Interstellar Preliminary Examination IX: High-speed interstellar dust analog capture in Stardust flight-spare aerogel. *Meteorit. Planet. Sci.* 10.1111/maps.12173 (2014).

18. V. J. Sterken *et al*., Stardust Interstellar Preliminary Examination X: Impact speeds and directions of interstellar grains on the Stardust dust collector. *Meteorit. Planet. Sci.* 10.1111/maps.12219 (2014).

19. R. M. Stroud *et al*., Stardust Interstellar Preliminary Examination XI: Identification and elemental analysis of impact craters on Al foils from the Stardust Interstellar Dust Collector. *Meteorit. Planet. Sci.* 10.1111/maps.12136 (2014).

20. A. J. Westphal *et al*., Final reports of the Stardust Interstellar Preliminary Examination. *Meteorit. Planet. Sci.* 10.1111/maps.12221 (2014).

21. Supplementary details are available on *Science* Online.

22. R. Lallement, J. L. Bertaux, On the decades-long stability of the interstellar wind through the solar system. *Astron. Astrophys.* **565**, A41 (2014). doi:10.1051/0004-6361/201323216

23. M. C. Price, A. T. Kearsley, M. J. Burchell, F. Hörz, J. Borg, J. C. Bridges, M. J. Cole, C. Floss, G. Graham, S. F. Green, P. Hoppe, H. Leroux, K. K. Marhas, N. Park, R. Stroud, F. J. Stadermann, N. Telisch, P. J. Wozniakiewicz, Comet 81P/Wild 2: The size distribution of finer (sub-10 μm) dust collected by the Stardust spacecraft. *Meteorit. Planet. Sci.* **45**, 1409–1428 (2010). doi:10.1111/j.1945-5100.2010.01104.x

24. M. C. Price, A. T. Kearsley, M. J. Burchell, L. E. Howard, J. K. Hillier, N. A. Starkey, P. J. Wozniakiewicz, M. J. Cole, Stardust interstellar dust calibration: Hydrocode modeling of impacts on Al-1100 foil at velocities up to 300 km s^{-1} and validation with experimental data. *Meteorit. Planet. Sci.* **47**, 684–695 (2012). doi:10.1111/j.1945-5100.2011.01300.x

25. A. T. Kearsley, J. Borg, G. A. Graham, M. J. Burchell, M. J. Cole, H. Leroux, J. C. Bridges, F. Hörz, P. J. Wozniakiewicz, P. A. Bland, J. P. Bradley, Z. R. Dai, N. Teslich, T. See, P. Hoppe, P. R. Heck, J. Huth, F. J. Stadermann, C. Floss, K. Marhas, T. Stephan, J. Leitner, Dust from comet Wild 2: Interpreting particle size, shape, structure, and composition from impact features on the Stardust aluminum foils. *Meteorit. Planet. Sci.* **43**, 41–73 (2008). doi:10.1111/j.1945-5100.2008.tb00609.x

26. A. J. Westphal, C. Snead, A. Butterworth, G. A. Graham, J. P. Bradley, S. Bajt, P. G. Grant, G. Bench, S. Brennan, P. Pianetta, Aerogel keystones: Extraction of complete hypervelocity impact events from aerogel collectors. *Meteorit. Planet. Sci.* **39**, 1375–1386 (2004). doi:10.1111/j.1945-5100.2004.tb00952.x

27. P. Tsou, D. E. Brownlee, S. A. Sandford, F. Horz, M. E. Zolensky, Wild 2 and interstellar sample collection and Earth return. *J. Geophys. Res. Planets* **108**, 8113 (2003). doi:10.1029/2003JE002109

28. S. A. Sandford, S. Bajt, S. J. Clemett, G. D. Cody, G. Cooper, B. T. Degregorio, V. De VERA, J. P. Dworkin, J. E. Elsila, G. J. Flynn, D. P. Glavin, A. Lanzirotti, T. Limero, M. P. Martin, C. J. Snead, M. K. Spencer, T. Stephan, A. Westphal, S. Wirick, R. N. Zare, M. E. Zolensky, Assessment and control of organic and other contaminants associated with the Stardust sample return from comet 81P/Wild 2. *Meteorit. Planet. Sci.* **45**, 406–433 (2010). doi:10.1111/j.1945-5100.2010.01031.x

29. J. P. Bradley, Chemically anomalous, preaccretionally irradiated grains in interplanetary dust from comets. *Science* **265**, 925–929 (1994). Medline doi:10.1126/science.265.5174.925

30. L. P. Keller, S. Messenger, On the origins of GEMS grains. *Geochim. Cosmochim. Acta* **75**, 5336–5365 (2011). doi:10.1016/j.gca.2011.06.040

31. P. C. Frisch, M. Bzowski, G. Livadiotis, D. J. McComas, E. Moebius, H. R. Mueller, W. R. Pryor, N. A. Schwadron, J. M. Sokół, J. V. Vallerga, J. M. Ajello, Decades-long changes of the interstellar wind through our solar system. *Science* **341**, 1080–1082 (2013). Medline doi:10.1126/science.1239925

32. V. Dikarev, E. Grün, M. Landgraf, W. J. Baggaley, D. P. Galligan, in *Proceedings of the Meteoroids 2001 Conference,* B. Warmbein, Ed. (2001), vol. 495, pp. 609–615.

33. M. Landgraf, M. Müller, E. Grün, Prediction of the in-situ dust measurements of the Stardust mission to comet 81P/Wild 2. *Planet. Space Sci.* **47**, 1029–1050 (1999). doi:10.1016/S0032-0633(99)00031-8

34. M. J. Burchell, M. J. Cole, M. C. Price, A. T. Kearsley, Experimental investigation of impacts by solar cell secondary ejecta on silica aerogel and aluminum foil: Implications for the Stardust Interstellar Dust Collector. *Meteorit. Planet. Sci.* **47**, 671–683 (2012). doi:10.1111/j.1945-5100.2011.01294.x

35. N. Gehrels, Confidence limits for small number events in astrophysical data. *Astrophys. J.* **303**, 336–346 (1986). doi:10.1086/164079

36. H. Krüger, E. Grün, Interstellar dust inside and outside the heliosphere. *Space Sci. Rev.* **143**, 347–356 (2009). doi:10.1007/s11214-008-9431-3

37. M. Min, J. W. Hovenier, L. B. F. M. Waters, A. de Koter, The infrared emission spectra of compositionally inhomogeneous aggregates composed of irregularly shaped constituents. *Astron. Astrophys.* **489**, 135–141 (2008). doi:10.1051/0004-6361:200809534

38. E. B. Jenkins, A unified representation of gas-phase element depletions in the interstellar medium. *Astrophys. J.* **700**, 1299–1348 (2009). doi:10.1088/0004-637X/700/2/1299

39. F. Kemper, W. J. Vriend, A. G. G. M. Tielens, The absence of crystalline silicates in the diffuse interstellar medium. *Astrophys. J.* **609**, 826–837 (2004). doi:10.1086/421339

40. F. Kemper, W. J. Vriend, A. Tielens, Errata: The absence of crystalline silicates in the diffuse interstellar medium (**609**, p. 826, 2004). *Astrophys. J.* **633**, 534–534 (2005). doi:10.1086/447764

41. A. P. Jones, J. A. Nuth III, Dust destruction in the ISM: A re-evaluation of dust lifetimes. *Astron. Astrophys.* **530**, A44 (2011). doi:10.1051/0004-6361/201014440

42. F. J. Molster, L. Waters, The mineralogy of interstellar and circumstellar dust. *Astromineralogy* **609**, 121–170 (2003). doi:10.1007/3-540-45840-9_3

43. S. Messenger, L. P. Keller, D. S. Lauretta, Supernova olivine from cometary dust. *Science* **309**, 737–741 (2005). Medline doi:10.1126/science.1109602

44. C. Vollmer, P. Hoppe, F. E. Brenker, C. Holzapfel, Stellar $MgSiO_3$ perovskite: A shock-transformed stardust silicate found in a meteorite. *Astrophys. J.* **666**, L49–L52 (2007). doi:10.1086/521623

45. B. T. Draine, Perspectives on interstellar dust inside and outside of the heliosphere. *Space Sci. Rev.* **143**, 333–345 (2009). doi:10.1007/s11214-008-9411-7

46. D. Nesvorny, P. Jenniskens, H. F. Levison, W. F. Bottke, D. Vokrouhlicky, M. Gounelle, Cometary origin of the Zodiacal cloud and carbonaceous micrometeorites. Implications for hot debris disks. *Astrophys. J.* **713**, 816–836 (2010). doi:10.1088/0004-637X/713/2/816

47. D. Nesvorny, D. Vokrouhlicky, W. F. Bottke, M. Sykes, Physical properties of asteroid dust bands and their sources. *Icarus* **181**, 107–144 (2006). doi:10.1016/j.icarus.2005.10.022

48. D. Jewitt, H. Weaver, J. Agarwal, M. Mutchler, M. Drahus, A recent disruption of the main-belt asteroid P/2010 A2. *Nature* **467**, 817–819 (2010). Medline doi:10.1038/nature09456

49. H. H. Hsieh, D. Jewitt, P. Lacerda, S. C. Lowry, C. Snodgrass, The return of activity in main-belt comet 133P/Elst-Pizarro. *Mon. Not. R. Astron. Soc.* **403**, 363–377 (2010). doi:10.1111/j.1365-2966.2009.16120.x

50. B. J. Gladman, D. R. Davis, C. Neese, R. Jedicke, G. Williams, J. J. Kavelaars, J.-M. Petit, H. Scholl, M. Holman, B. Warrington, G. Esquerdo, P. Tricarico, Sub-Kilometer Asteroid Diameter Survey (SKADS) V1.0. EAR-A-I0655-5-SKADS-V1.0. NASA Planetary Data System (2010).

51. E. Grün, H. A. Zook, H. Fechtig, R. H. Giese, Collisional balance of the meteoritic complex. *Icarus* **62**, 244–272 (1985). doi:10.1016/0019-1035(85)90121-6

52. R. L. Smith, K. M. Pontoppidan, E. D. Young, M. R. Morris, E. F. van Dishoeck, High-precision (CO)-O-17, (CO)-O-18, and (CO)-O-16 measurements in young stellar objects: Analogues for CO self-shielding in the early solar system. *Astrophys. J.* **701**, 163–175 (2009). doi:10.1088/0004-637X/701/1/163

53. E. D. Young, M. Gounelle, R. L. Smith, M. R. Morris, K. M. Pontoppidan, Astronomical oxygen isotopic evidence for supernova enrichment of the solar system birth environment by propagating star formation. *Astrophys. J.* **729**, 43 (2011). doi:10.1088/0004-637X/729/1/43

54. L. R. Nittler, E. Gaidos, Galactic chemical evolution and the oxygen isotopic composition of the solar system. *Meteorit. Planet. Sci.* **47**, 2031–2048 (2012). doi:10.1111/j.1945-5100.2012.01410.x

55. J. G. A. Wouterloot, C. Henkel, J. Brand, G. R. Davis, Galactic interstellar $^{18}O/^{17}O$ ratios - a radial gradient? *Astron. Astrophys.* **487**, 237–246 (2008). doi:10.1051/0004-6361:20078156

56. A. A. Penzias, The isotopic abundances of inter-stellar oxygen. *Astrophys. J.* **249**, 518–523 (1981). doi:10.1086/159311